S41B-2186: A review of the virtual refraction and application to active source and crustal imaging

T. Dylan Mikesell*, Kasper van Wijk* and Elmer Ruigrok†

*Physical Acoustics Lab and Department of Geosciences, Boise State University, 1910 University Dr., Boise, ID 83725
†Department of Geotechnology, Delft University of Technology, Stevinweg 1, 2628 CN, Delft, The Netherlands

Abstract

We present an overview of the spurious arrival in seismic interferometry called the virtual refraction. We find that this artifact is present in the crosscorrelated wavefields when refractions are present in the input data and can be used to characterize the subsurface velocity structure. In crustal seismic studies, refracted Pg, Pn and P_{diff} phases are often used in a tomographic sense to create a subsurface velocity model that defines the geologic structure. We apply the virtual refraction analysis to synthetic data with varying near-surface thickness. In this analysis, we look at the effects crosscorrelation on a modified *delay-time* method to estimate receiver statics. We then crosscorrelated P_{diff} phases from earthquakes to estimate receiver-side traveltime anomalies in the western United States.

1. The virtual refraction

The Green's function between two receivers is obtained by crosscorrelating the recorded wavefields from sources located on an enclosing surface around the receivers (*Wapenaar and Fokkema*, 2006). In exploration seismics, this technique is often called seismic interferometry (SI). In field data applications, an artefact related to head waves is often present when the original data contain head waves. We call this spurious event the *virtual refraction*.

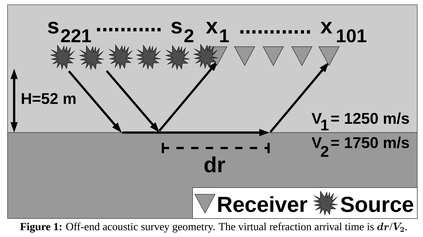

Figure 1: Off-end acoustic survey geometry. The virtual refraction arrival time is dr/V_2.

Figure 1 shows the geometry for a numerical off-end acoustic experiment. The shot record for a source at X_1 is shown in Figure 2 (left). If we crosscorrelate the wavefield at X_1 with all other receivers and sum over each source we create the virtual shot record in Figure 2 (right). Only the direct wave and virtual refraction are present because they have stationary phase points. The moveout of the virtual refraction defines the refractor velocity in the horizontal layers case.

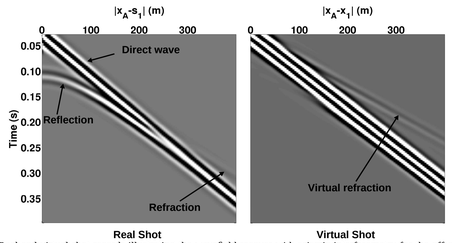

Figure 2: Real and virtual shot records illustrating the wavefield recover with seismic interferometry for the off-end acoustic survey in Figure 1.

2. Delay-time statics

Small perturbations due to near-surface heterogeneity deteriorate the final reflection seismic image. Figure 3 shows an example of a near surface model where the weathering layer varies in thickness laterally. A variety of methods exist to correct for this type of near-surface heterogeneity. For example, if the weathering layer velocity is known, elevation statics can be computed and the recorded seismic traces can be corrected.

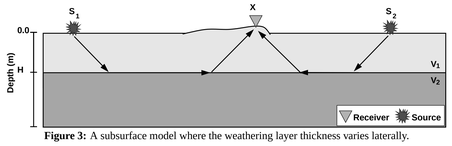

Figure 3: A subsurface model where the weathering layer thickness varies laterally.

In areas where the weathering velocity is not known, other methods, many based on first-break analysis, have been developed to estimate static time shifts that correct the travel time perturbation at each source or receiver. One such method is the *delay-time* method (e.g., p. 120 in *Burger et al.*, 2006). In the *delay-time* method, the refracted arrival time T_{SX} is

$$T_{SX} = T_S + T_X + \frac{|S - X|}{V_2}, \tag{1}$$

where $|S - X|$ is the distance between the source (S) and receiver (X) and V_2 is the refractor velocity. T_S and T_X are delays associated with near-surface heterogeneity along the ray, either near the source or receiver, respectively. In this approach V_2, T_S and T_X can be estimated if sources exists on each side of the receiver, which corrects for dipping interfaces.
For a source on each side of X (Figure 3) we have two arrival time equations:

$$\begin{aligned} T_{S_1X} &= T_{S_1} + T_X + \frac{|S_1 - X|}{V_2} \\ T_{S_2X} &= T_{S_2} + T_X + \frac{|S_2 - X|}{V_2}. \end{aligned} \tag{2}$$

We can represent this system of equations in matrix notation such that $d = AM$, where d is the matrix of observed arrival times $T_{S_iX_j}$, $i = 1, ..., n$ and $j = 1, ..., m$ for n sources and m receivers. m is the model vector, containing delay times for each source and receiver as well as V_2. We can linearly invert this system of equations to estimate the delay for each source and receiver following $m = A^{\dagger}d$, $A^{\dagger}$ is the inverse of A, which can be estimate from a variety of techniques. This approach assumes the that refractor surface is planar and that the path along the refractor is equivalent to distances $|S_i - X_j|$ at the surface.

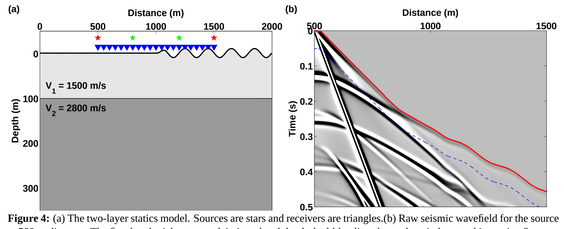

Figure 4: (a) The two-layer statics model. Sources are stars and receivers are triangles.(b) Raw seismic wavefield for the source at 500 m distance. The first-break picks are overlain in red and the dashed-blue line shows the window used in section 3.

We test the *delay-time* method with a numerical 2D seismic experiment. We create vertical component synthetic seismic data for the model in Figure 4a using the Spectral Element Method (*Komatitsch and Vilotte*, 1998). On the left half of the model, the near-surface has a constant thickness of 100 m. On the right side, the near-surface thickness varies as a sine wave with a peak-to-peak variation of 20 m. We show the shot record from the source at 500 m distance in Figure 4b. We use the modified-energy ratio (MER) method (*Han et al.*, 2008) to pick first breaks (red line).

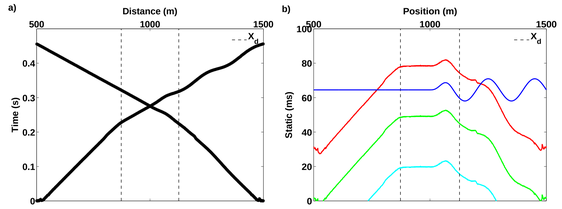

Figure 5: (a) The first-break data used to compute the *delay-time* static. (b) *delay-time* static using shots on each end of receiver array. The dashed lines indicate the cross-over distances, within which, the refraction is the first arrival.

Using the first breaks from the shots on both ends of the receiver array (Figure 5a), we invert the system of travel time equations to estimate a delay time for both sources and each receiver (Figure 5b) (cyan line). We estimate the refractor velocity, V_2=2210 m/s. Redatuming to the refractor, we estimate the total static (blue line) that we should apply the receivers. The *delay-time* method offers a static that is split amongst the receivers, sources and the estimate of V_2. This method underestimates the refractor velocity by 22%. That underestimation effects the delay-time estimates. We superpose the left side source static (green line) and right side source static (red line) in order to estimate a complete static. We see that we get close to the correct static, but because we inaccurately estimate V_2 we do not estimate the total static. The black-dashed lines indicate the crossover distance, where the refractions in (a) are the first arrivals. As visible in (b), the *delay-time* method does not correctly estimate structure outside of this area (e.g., p. 126 in *Burger et al.*, 2006). In the next section we present a modified *delay-time* method that incorporates the virtual refraction.

3. Modified delay-time statics with the VR

What happens if we estimate the virtual refraction using seismic interferometry and then apply the *delay-time* method? Consider two receivers at X_A and X_B. Similar to the delay time method, we represent the refraction arrival at each receiver as

$$\begin{aligned} T_{SX_A} &= T_S + T_{X_A} + \frac{|S - X_A|}{V_2} \\ T_{SX_B} &= T_S + T_{X_B} + \frac{|S - X_B|}{V_2}. \end{aligned} \tag{3}$$

Crosscorrelating the refracted arrivals at X_A and X_B we eliminate the shared parts of the raypath

$$T_{SX_A} - T_{SX_B} = T_{X_A} - T_{X_B} + \frac{|X_B - X_A|}{V_2}. \tag{4}$$

Assuming that the weathering layer velocity is constant, this crosscorrelation is the virtual refraction, plus the travel time perturbation $\Delta T = T_{X_A} - T_{X_B}$. ΔT is the static at X_A relative to the reference receiver X_B. We have eliminated the source static through crosscorrelation. The red raypaths in Figure 6 represent the crosscorrelation results (i.e., the virtual refraction containing a small travel time perturbation.

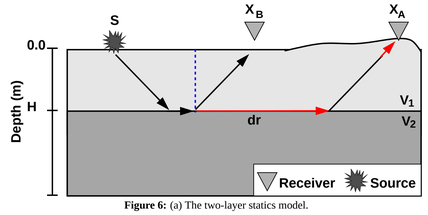

Figure 6: (a) The two-layer statics model.

To generate the virtual refraction, we crosscorrelate the receiver at the green star on the left with every other receiver for the source on the left. We do the same thing to the right hand side. However, before we crosscorrelate we window around the first breaks to suppress crosscorrelation of other events. In this way, we crosscorrelate either the direct wave or the refraction. Figure 7a and b shows the estimated virtual shot records for virtual sources at 800 and 1200 m, respectively.

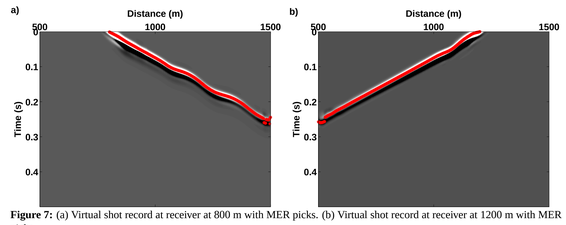

Figure 7: (a) Virtual shot record at receiver at 800 m with MER picks. (b) Virtual shot record at receiver at 1200 m with MER picks.

We see that the first arrival is now the virtual refraction rather than the direct wave. We plot the first-break picks in Figure 8a. The dashed blue lines now represent the data domain in which the virtual refraction is the first arrival. Within this range, we should expect the *modified delay-time* method to estimate a static with the correct structure.

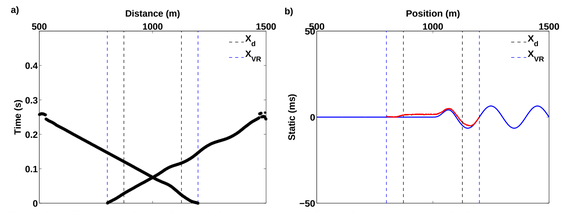

Figure 8: (a) The virtual refraction first-break data used to compute the *modified delay-time* static. (b) *delay-time* static using shots on each end of receiver array.

The static is now relative to the reference stations (i.e., X=800 or 1200 m), which are both at the same thickness. We plot the static estimated with the *modified delay-time* method in Figure 8 (red line). The true static is the blue line. We see that within the blue dashed lines, the magnitude and structure of the near-surface static are well estimated. The refractor velocity in this case is also improved compared to the original *delay-time* method, V_2=2765 m/s. This estimate is underestimated by 1%, a significant improvement.

4. Future work: isolating mantle heterogeneity

When we do not have sources on both sides of the receiver array, or when the velocity model above the refractor is not homogeneous, we can use the P_{diff} virtual refraction to isolate which part of the Earth contains heterogeneity. The following example shows how we can use ΔT estimates to highlight structure within the crust and mantle below USArray.

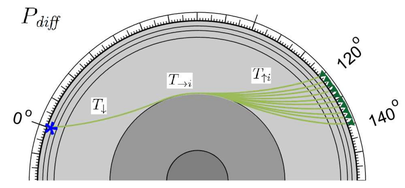

Figure 9: A half-section of the Earth showing P_{diff} arrivals. The raypaths between one source (blue star) and an array of receivers (green triangles) are indicated. The traveltime segments at the source-side, along the diffractor (CMB), and at the receiver-side are denoted with $T_{\downarrow}$, $T_{-\downarrow i}$ and $T_{\uparrow i}$, respectively, where $_i$ is a receiver index.

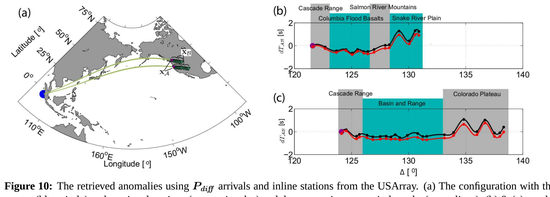

Figure 10: The retrieved anomalies using P_{diff} arrivals and inline stations from the USArray. (a) The configuration with the source (blue circle) and receiver locations (green triangles) and the connecting great-circle paths (green lines). (b) & (c) are the receiver-side traveltime anomalies for the northern and southern subarrays, respectively. The points are the extracted anomalies at the different stations; the lines are created through spline interpolation of the points. The black and red lines denote the functions with and without static correction, respectively. In (a) the reference stations are colored purple. In (b) & (c) the data points for the reference stations are highlighted in purple. By definition, the traveltime anomalies at the reference stations are zero.

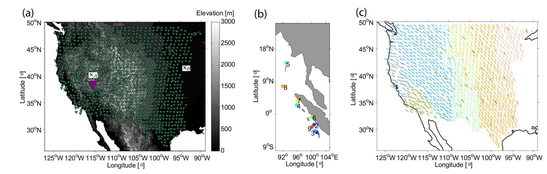

Figure 11: (a) The distribution of USArray stations used in this study (green triangles) projected onto a topographic map of part of the USA. The reference station at position x_A is indicated by the purple triangle. (b) The locations of the 9 earthquakes used to make the anomaly map (Fig. 12a). (c) Illumination map–the colored lines denote the backazimuth to the earthquakes in (b). In (b) and (c) the same colors are used.

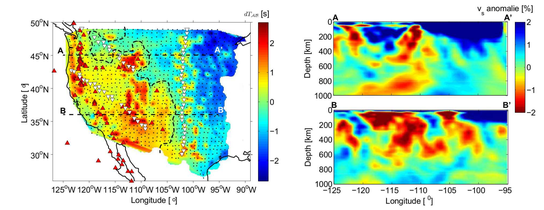

Figure 12: (a) Mantle-crust anomaly map imaged using the new P_{diff} traveltime-difference method. We have labeled 1) the primarily Holocene volcanism (red triangles, source: http://www.volcano.si.edu/); 2) the interpreted boundary between slow (west side) and fast (east side) lithosphere (undulating dashed line); 3) the location of two cross-sections A-A' and B-B' (dashed straight lines); 4) USArray stations used in this study (black dots); 5) the station locations used in Fig. 10 (NE-SW subarrays of white triangles). (b) and (c) are v_s anomaly sections along A-A' and B-B', at 45^0 and 36^0 latitude, respectively. These are extracted from the DNA10-S model (*Obrebski et al.*, 2011).

5. Conclusion

- Spurious head waves in applications of seismic interferometry are often present because requirements for exact recovery of the Green's function between receivers cannot be met in practice.
- For horizontal layers, we can estimate the velocity of the faster layer from the slope of the virtual refraction.
- For varying near-surface layers we can estimate the refractor velocity and receiver statics using a modified *delay-time* inversion based on the virtual refraction first breaks.
- We can crosscorrelate CMB refractions (P_{diff}) to isolate receiver-side heterogeneity within the crust & mantle.
- This is a fast and simple technique to determine areas of increased sub-surface structure.

Acknowledgments

E.R is supported by The Netherlands Organization for Scientific Research (NWO). The facilities of the IRIS Data Management System, and specifically the IRIS Data Management Center, were used for access to waveform and metadata required in this study. Data from the TA network were made freely available as part of the EarthScope USArray facility supported by the National Science Foundation, Major Research Facility program under Cooperative Agreement EAR-0350030. We thank the developers of SPECFEM2D numerical modeling software.

References

Burger, H. R., A. F. Sheehan, and C. H. Jones (2006), *Introduction to Applied Geophysics: Exploring the Shallow Subsurface*, W. W. Norton & Company.

Han, L., J. Wong, J. C. Bancroft, and R. R. Stewart (2008), Automatic time picking and velocity determination on full waveform sonic well logs, *Tech. Rep. 20*, CREWES, University fo Calgary.

Komatitsch, D., and J.-P. Vilotte (1998), The spectral element method: An efficient tool to simulate the seismic response of 2d and 3d geological structures, *Bull. Seism. Soc. Am.*, *88*(2), 368–392.

Obrebski, M., R. M. Allen, F. Pollitz, and S. Hung (2011), Lithosphere-asthenosphere interaction beneath the western United States from the joint inversion of body-wave traveltimes and surface-wave phase velocities, *Geophysical Journal International*, *185*(2), 1003–1021, doi: 10.1111/j.1365-246X.2011.04990.x.

Snieder, R., K. van Wijk, M. Haney, and R. Calvert (2008), Cancellation of spurious arrivals in Green's function extraction and the generalized optical theorem, *Phys. Rev. E*, *78*, 036,606, doi:10.1103/PhysRevE.78.036606.

Wapenaar, K., and J. Fokkema (2006), Green's function representations for seismic interferometry, *Geophysics*, *71*(4), S133–S146, doi:10.1190/1.2213955.

author email: dmikesell@cgiss.boisestate.edu **AGU FALL MEETING 2011**